

3D Multiple Input Single Output Near Field Automotive Synthetic Aperture Radar

Aron Sommer*, Tri Tan Ngo*, Jörn Ostermann*

*Institut für Informationsverarbeitung
Appelstr. 9A, D-30167 Hannover, Germany
email: sommer@tnt.uni-hannover.de,
ngo@tnt.uni-hannover.de,
ostermann@tnt.uni-hannover.de

Abstract: Radar sensors play an important role in the technology field of autonomous driving. In contrast to optical cameras, they work reliable by night, mist, snow and fog. Recent radar sensors have problems in near-field scenarios. In this paper, we investigate how the technique of synthetic aperture radar (SAR) can be used to reconstruct the 3D near-field environment up to 30 m with several physical radar sensors using the global backprojection algorithm. The main challenge applying SAR to an automotive 77 GHz radar sensor with 2 GHz bandwidth and a short sweep duration of 10 μ s is to avoid azimuth aliasing, which means avoiding ghost targets. In the case of monostatic SAR, the sensors have to be placed 1 mm next to each other, which is unrealistic in practice. By using multiple input single output (MISO) sensors arranged in a circular manner we increase this distance to 4 cm, which is now feasible in practice. This sensor arrangement enables applying SAR to near-field automotive applications.

1. Introduction

Autonomous driving is one of the main objectives of the 21st century. Currently, sensor fusion is pursued by many automotive manufacturers, where for example cameras and radar sensors are combined to improve advanced driver assistance systems. Optical cameras have the advantage that their signals can be evaluated to provide scene understanding, like reading road signs. Furthermore, radar sensors measure the distance to objects in all weather conditions and even by night. In general, radar sensors transmit electromagnetic waves and receive their scattered echoes. Frequency modulated continuous waves (FMCW) [1] are often used in near-field scenarios. To reduce the impact of moving targets, which shifts the signal spectrum due to their velocity, rapid chirps [1, 2] are used in automotive radar systems. Due to their extreme short sweep time, the Doppler effect in radar measurements can be neglected. Current radar systems [3] use a carrier frequency of 77 GHz and a bandwidth of 2 GHz. These parameters yield a range resolution of approximately 7.5 cm. On the contrary, these radar systems use a small antenna beam to evaluate different beam angles. Hence, this approach leads to a coarse angular resolution.

Synthetic aperture radar [4] is an imaging technique, which uses a wide beam antenna to generate high angular resolution radar images. It moves a radar sensor along a straight line and

takes several radar measurements. Applying this technique to automotive radar applications means moving the sensor mechanically at the front of a car, which is not desirable. To prevent the mechanical component, forward-looking SAR [5] with several antennas instead of one moving antenna can be used. Even forward-looking SAR with multiple receive antennas [6] is investigated for airborne radar systems. These approaches work reliably in far-field. Near-field 3D SAR systems [7] use one sensor mounted on a rotating disk to guarantee dense equidistant sampling. This strategy has again a mechanically moving component.

This paper shows the applicability and capability of 3D synthetic aperture radar to automotive applications. We demonstrate that the ambiguity problem can be solved by multiple input single output (MISO) sensor arrays without any moving components.

We show that for a monostatic radar system the antenna elements have to be placed maximal 1 mm next to each other, which is unrealistic in practice. A larger distance between the antenna elements would result in azimuth aliasing and ghost targets. This problem is also known as the ambiguity problem. However, using MISO antennas, placed in a specific 2D manner, avoid azimuth aliasing and generate high-resolution 3D mappings of the surrounding. We compare different antenna geometries and show that the circular antenna arrangement allows a distance of 4 cm between the antennas without any loss of image quality. Furthermore, we extend the global backprojection algorithm to process the MISO raw data.

This article is structured as follows: In Section 2 the fundamentals of FMCW signals and rapid chirps are given. A short introduction to the idea of synthetic aperture radar is also presented in Section 2. Section 3 shows the azimuth aliasing problem. The extended global backprojection algorithm and the main investigations are presented in Section 4. Section 5 gives experimental results of a road traffic simulation. This article ends with a conclusion in Section 6.

2. Signal Model and Algorithm

In this section *Frequency Modulated Continuous Wave* (FMCW) signals are described mathematically. Afterward, we give a short introduction to *rapid chirps* and to the standard *global backprojection* algorithm.

2.1. Frequency Modulated Continuous Waves (FMCW)

Near-field FMCW systems [8] typically use *chirp* signals to measure distances. A chirp signal has a linear modulation of time and is expressed as the complex signal

$$s(t) = \text{rect}\left(\frac{t}{T} - \frac{1}{2}\right) \cdot \exp(2\pi i(f_c t + \frac{1}{2}\alpha t^2)),$$

where t is the time variable, f_c the carrier frequency, α the chirp rate and i the imaginary unit. The chirp rate $\alpha = B/T$ is the transmitted bandwidth B over the sweep duration T of a single chirp, see Figure 1. Note that using rapid chirps means choosing T to be very small. A typical FMCW signal consists of a concatenation of chirp signals.

For the sake of simplicity, we assume that in the following the transmitted signal is scattered only by one point target. The backscattered signal s_r is received by the same radar sensor and has a time difference τ , which is proportional to the two-way propagation distance:

$$s_r(t) = \text{rect}\left(\frac{t-\tau}{T} - \frac{1}{2}\right) \cdot \exp\left(2\pi i(f_c(t-\tau) + \frac{1}{2}\alpha(t-\tau)^2)\right).$$

The complex conjugated signal s_r^* is multiplied by the transmitted signal s , which is in practice implemented as a mixer and a low-pass filter, in order to get the beat signal

$$\begin{aligned} s_b(t) &= s(t) \cdot s_r^*(t) \\ &= \text{rect}\left(\frac{t}{T} - \frac{1}{2}\right) \cdot \exp\left(2\pi i(f_c\tau + \alpha t\tau - \frac{1}{2}\alpha\tau^2)\right). \end{aligned}$$

We compute the Fourier Transform of the beat signal s_b and convert the frequency variable to its time delay $f = \alpha t$ to get the *range compressed data* [8]

$$d(t) = \exp\left(2\pi i(f_c\tau - \frac{1}{2}\alpha\tau^2)\right) \cdot \exp(-\pi i\alpha t) \cdot T \text{sinc}(B(t - \tau)). \quad (1)$$

For more than one point reflectors, the data d can be computed by the superposition of the signals of each point reflector [9].

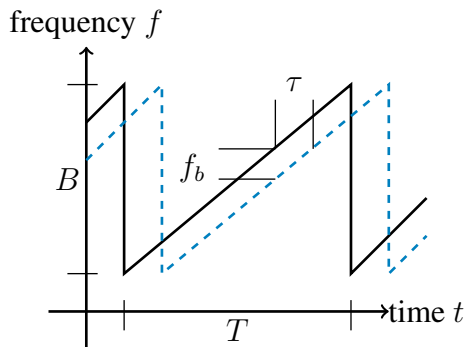


Figure 1: Principal of FMCW radar. The black continuous line represents the transmitted signal frequencies, whereas the blue dashed line stands for the received frequencies. The radar has a bandwidth B and a sweep duration T . The time delay τ results in the beat frequency f_b .

2.2. Rapid Chirps

Modern automotive radar sensors use rapid chirps [1, 2] to reduce the impact of the Doppler effect in measurements, which results from moving targets. By using an extreme short sweep time T , for instance $T = 10 \mu\text{s}$, the movement of an object during one sweep is very small. Hence, it can be assumed that all objects in the scene are static. In the following, we derive the maximal allowed speed of targets.

Let a single point target has a radial velocity denoted by v_r . The radial velocity can be neglected, if the traveled distance of the target during one sweep is less than the range resolution Δr of the radar sensor [8, 10]:

$$|v_r| \cdot T \leq \Delta r.$$

Using the resolution equation $\Delta r = c/(2B)$ of a FMCW system leads to the upper bound [8, 10]

$$|v_r| \leq \frac{\Delta r}{T} = \frac{c}{2TB}.$$

For a bandwidth of $B = 2 \text{ GHz}$ and a sweep duration of $T = 10 \mu\text{s}$ the maximal permitted relative radial velocity of a moving object is

$$|v_r| \leq \frac{c}{2TB} = \frac{3 \cdot 10^8 \text{ m/s}}{2 \cdot 10^{-5} \text{ s} \cdot 2 \cdot 10^9 \text{ 1/s}} \approx 2083 \text{ km/h}.$$

Hence, rapid chirps allow the assumption that in practice all targets in the scene are static.

2.3. Synthetic Aperture Radar - Global Backprojection

In general, a radar sensor measures radial distances to all objects in the illuminated scene. By moving the radar along a straight line and taking measurements at many equidistant positions, a radar image can be formed [11]. The phase centers of the equidistant sensor positions are the *aperture positions*. This technique is called synthetic aperture radar (SAR) [4].

In this work we use several small sensors, one at each aperture position. Sequentially, each sensor transmits a chirp signal and receives their echoes, whereas all other sensors go to sleep. Here we use the global backprojection algorithm based on Gorham's implementation [12] to generate a SAR image, because it has the capability to process arbitrary antenna geometries. The global backprojection algorithm can be expressed mathematically by the following equation, where the intensity I of a pixel at $\mathbf{x} \in \mathbb{R}^2$ is computed by

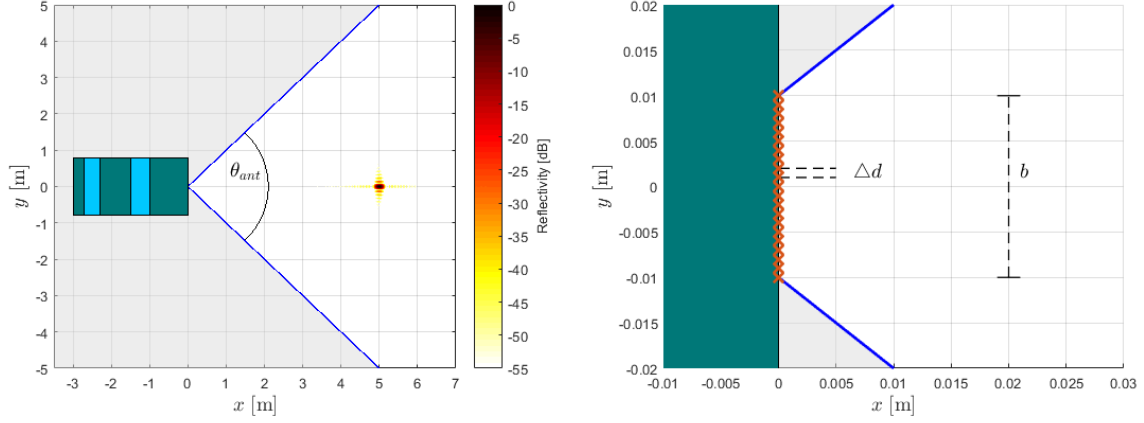
$$I(\mathbf{x}) = \sum_{l=1}^N d_l \left(\frac{2\|\gamma_l - \mathbf{x}\|_2}{c} \right) \cdot \exp \left(2\pi i f_c \frac{2\|\gamma_l - \mathbf{x}\|_2}{c} \right).$$

The aperture positions are denoted by γ_l for $l = 1 \dots N$. The range compressed data d_l is measured by antenna l and can be described by Equation (1).

Figure 2 shows a simulation, which visualizes the concept of 2D SAR. In Figure 2 (a) the car itself, where the antenna is mounted at the front, is shown. The blue lines visualize the $\theta_{\text{ant}} = 90^\circ$ illumination angle of the sensor. The point reflector, which is reconstructed precisely by the global backprojection algorithm, is 5 m in front of the car. Figure 2 (b) shows the antenna arrangement in detail. The aperture positions along a straight line are marked by red crosses.

3. Aliasing in Azimuth - Impact of the Distance between Aperture Positions

In the field of synthetic aperture radar, it is well known that there exists an upper bound \bar{d} of the distance Δd between the aperture positions [4]. If Δd is greater than the upper bound \bar{d} , ghost targets appear in the SAR image because of ambiguities, see Figure 3. The Shannon sampling



(a) Precise 2D reconstruction.

(b) Aperture positions with distance $\Delta d = 1$ mm and width $b = 2$ cm.

Figure 2: (a) Car and illuminated area of 90° , marked by blue lines. The precisely reconstructed point reflector is 5 m in front of the car. (b) Enlarged section of the radar antenna at the front of the car. The red crosses mark the aperture positions. Here no aliasing occurs, because $\Delta d < \bar{d}$.

theorem in azimuth is violated. To avoid these ghost targets, the distance Δd must fulfill the azimuth sampling formula [4]

$$\Delta d < \bar{d} = \frac{c}{1.2 \cdot (f_c + \frac{B}{2}) \cdot \theta_{\text{ant}}}. \quad (2)$$

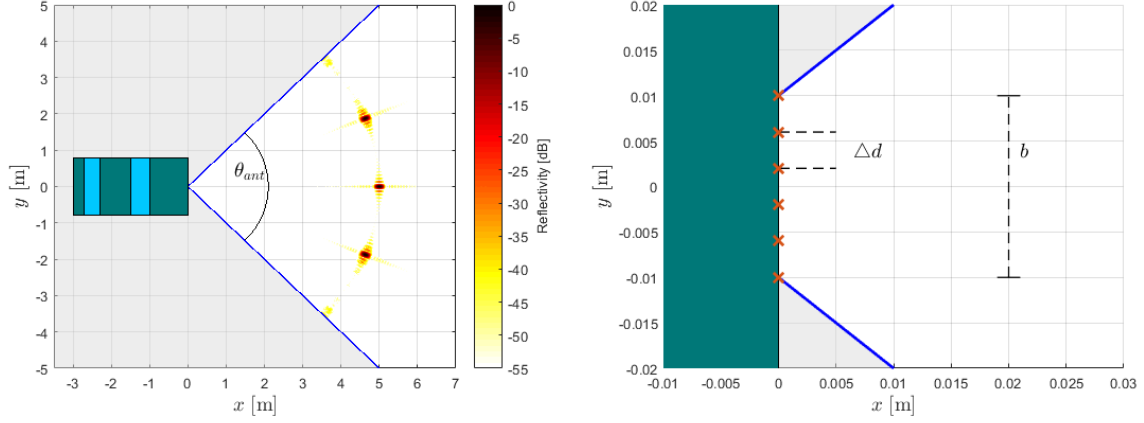
An oversampling factor of 1.2 in inequality (2) is typically used in SAR systems [4] for stability. In an automotive scenario [4] with a carrier frequency of $f_c = 77$ GHz, a bandwidth of $B = 2$ GHz and an illumination angle of $\theta_{\text{ant}} = 90^\circ$ we get the upper bound

$$\bar{d} = \frac{3 \cdot 10^8 \text{ m/s}}{1.2 \cdot (77 + \frac{2}{2}) \cdot 10^9 \text{ Hz} \cdot \frac{\pi}{2}} = 1 \text{ mm}.$$

This means, if we want to map $\theta_{\text{ant}} = 90^\circ$ in front of our radar system, the distance between the aperture positions must be less than $\bar{d} = 1$ mm to avoid ghost targets.

A larger distance, for instance $\Delta d = 4$ mm in Figure 3 (b), leads to the ghost targets in Figure 3 (a). It shows the effect of azimuth aliasing in case of one point reflector. The global backprojection algorithm reconstructs three reflectors inside the illuminated area. Two of them are ghost targets. The real true reflector is again 5 m in front of the car, compare Figure 2.

To sum up, this investigation shows mathematically and by a simulation that in a near-field automotive SAR scenario the distance between the aperture positions has to be less than 1 mm. In practice, this requirement is unrealistic, because a simple patch antenna has usually a minimal length and width of $\lambda/2$, where $\lambda = 3.9$ mm is the wavelength. Hence, it is not possible to place these sensors next to each other and simultaneously to satisfy the aliasing Equation (2).



(a) 2D reconstruction with ghost targets.

(b) Aperture positions with distance $\Delta d = 4$ mm and width $b = 2$ cm.

Figure 3: (a) Car and illuminated area of 90° , marked by blue lines. The true point reflector is 5 m in front of the car. Ghost targets exist, because azimuth aliasing occurs. (b) Enlarged section of the radar antenna. The red crosses mark the aperture positions. Here $\Delta d > \bar{d}$.

4. 3D MISO SAR and its SISO Representation with Synthetic Antennas

We solve the problem of a not feasible, too small distance between the antenna apertures by applying the principle of multiple input single output (MISO) antenna technology. MISO antennas transmit a signal from only one antenna and receive the scattered echoes with all antennas in the antenna array. MISO antennas along a straight line, see Figure 3 (b), do not lead to the desired effect. Thus, we increase the degrees of freedom and perform a 3D reconstruction. Hence, we place the antennas elements on a plane instead of along a straight line.

For MISO SAR the global backprojection algorithm has to be modified, because the transmitter and the receiver are not the same antenna anymore. Additionally, the intensity I of a pixel at $\mathbf{x} \in \mathbb{R}^3$ depends now on the signals of every combination of all transmitter and receiver. This is mathematically described by [4]

$$I(\mathbf{x}) = \sum_{l=1}^N \sum_{k=1}^N d_{l,k} \left(\frac{\|\gamma_l - \mathbf{x}\|_2 + \|\gamma_k - \mathbf{x}\|_2}{c} \right) \cdot \exp \left(2\pi i f_c \frac{\|\gamma_l - \mathbf{x}\|_2 + \|\gamma_k - \mathbf{x}\|_2}{c} \right),$$

where γ_l and γ_k denote the aperture positions of antenna l and antenna k . The data $d_{l,k}$ is the range compressed data, which is measured by antenna k , when antenna l transmits a chirp.

With the extended 3D MISO backprojection algorithm we increase the distance between aperture positions without violating the azimuth aliasing Equation (2). However, to illustrate the azimuth aliasing in a multiple input single output (MISO) antenna network, we introduce the concept of synthetic antennas. The position of a physically real antenna is denoted by $\gamma_{\text{real}}^l \in \mathbb{R}^3$ for $l = 1, \dots, N$ and the position of a synthetic antenna by $\gamma_{\text{syn}}^j \in \mathbb{R}^3$ for $j = 1, \dots, N^2$.

We define the position of a synthetic antenna to be in the middle of two real antennas:

$$\gamma_{\text{syn}}^j = \frac{\gamma_{\text{real}}^l + \gamma_{\text{real}}^k}{2}, \quad \text{for all } l, k = 1, \dots, N.$$

Thus, the data, transmitted by antenna l , scattered at some object and received by antenna k , is approximately the same data, which would be transmitted and received by the synthetic antenna j . This assertion is based on the approximation

$$2 \|\gamma_{\text{syn}}^j - \gamma_{\text{obj}}\|_2 \approx \|\gamma_{\text{real}}^l - \gamma_{\text{obj}}\|_2 + \|\gamma_{\text{real}}^k - \gamma_{\text{obj}}\|_2, \quad (3)$$

which holds, if the distance between γ_{real}^l and γ_{real}^k is much smaller than the distance $\|\gamma_{\text{syn}}^j - \gamma_{\text{obj}}\|_2$. Figure 4 visualizes approximation (3). Hence, the proposed 3D MISO extended backprojection algorithm yields approximately to the same 3D reconstruction as the standard SISO global backprojection algorithm with its corresponding synthetic antennas.

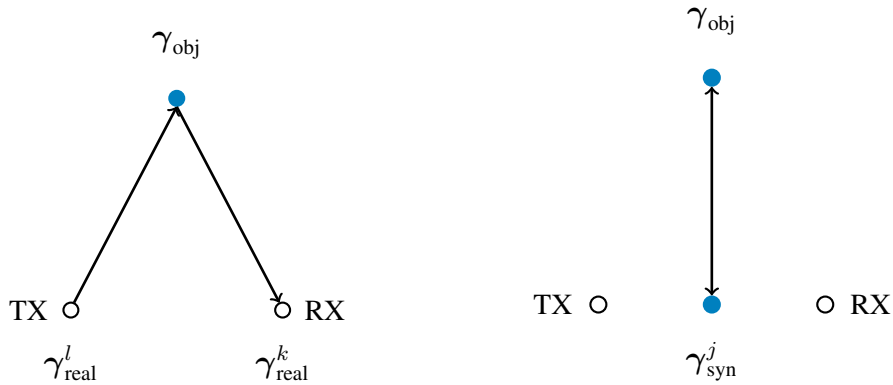


Figure 4: Idea of synthetic antennas. The transmit antenna is denoted by TX. The acronym RX stands for the receive antenna. The distance from TX located at γ_{real}^l to the object at γ_{obj} and back to RX at γ_{real}^k is approximately the same as the two way distance from the synthetic antenna at γ_{syn}^j to the object.

Consequently, in a MISO radar system, the synthetic antennas have to satisfy the aliasing Equation (2), which means that the distance between the real antennas can be greater than 1 mm. This result is the main contribution of this paper.

We verify by some numerical investigations that the distance between the aperture positions can be increased up to 4 cm. Additionally, we find the best 2D antenna arrangement. Accordingly, we simulate different antenna arrangements of a cross, some symmetric polygons and a circle, which are in total 50 cm long and 50 cm wide. One point reflector is placed 5 m in front of the car. The system has a carrier frequency of $f_c = 77$ GHz, a bandwidth of $B = 2$ GHz and an illumination angle of $\theta_{\text{ant}} = 90^\circ$.

Some of the results, especially the arrangements of the real antennas, their synthetic antennas and the reconstructions by the extended backprojection algorithm can be seen in Figure 5. The 3D reconstructions are visualized by isosurfaces at -7 dB. It can clearly be seen that for a circular MISO antenna no ghost targets occurs in the image, whereas in the other cases multiple ghost targets are visible.

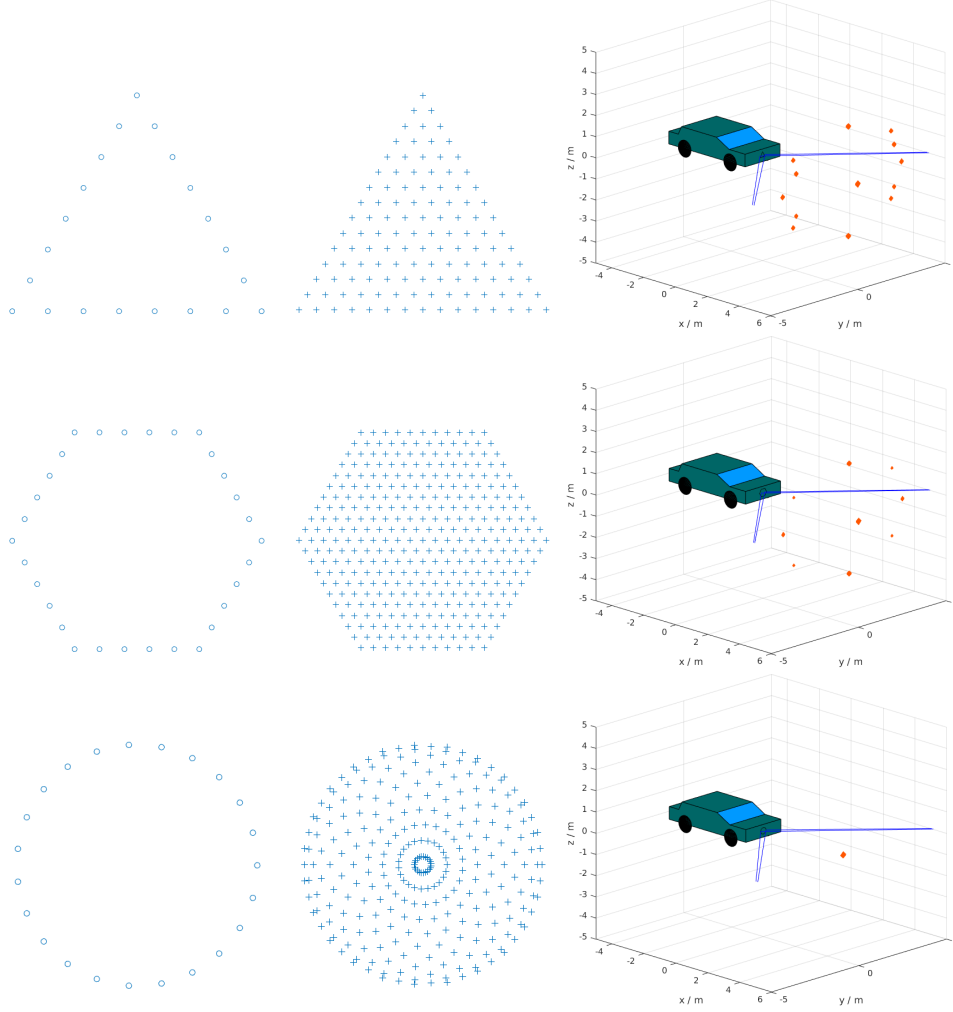


Figure 5: Results for triangle, hexagon and circle antenna. Left side: Real antennas. Middle column: Corresponding synthetic antennas. Right side: -7 dB isosurfaces of 3D Reconstruction.

To analyze the image quality resulting from more than the in Figure 5 shown antennas we count the number of ghost targets, measure the 3D *integrated side lobe ratio* (ISLR) [13] and the 3D *peak side lobe ratio* (PSLR) [13]. The ISLR is defined by

$$\text{ISLR} = 10 \log_{10} \left(\frac{P(4 \cdot \delta_r) - P(\delta_r)}{P(\delta_r)} \right), \quad \text{where} \quad P(\delta_r) = \int_{\mathcal{B}_{\delta_r}} |I(\mathbf{x})|^2 d\mathbf{x}.$$

Here, \mathcal{B}_{δ_r} denotes a ball with radius δ_r , centered at the position of the point reflector. The radius δ_r is chosen to be the spatial resolution of the radar system.

The PSLR indicates the ratio of the maximal absolute intensity in the side lobe to the maximal absolute main lobe intensity of the reconstruction of one point reflector. It is computed by

$$\text{PSLR} = 10 \log_{10} \left(\frac{I_S}{I_M} \right), \quad \text{where} \quad I_M = \max_{\mathbf{x} \in \mathcal{B}_{\delta_r}} \{|I(\mathbf{x})|\}, \quad I_S = \max_{\mathbf{x} \in \mathcal{B}_{4 \cdot \delta_r} \setminus \mathcal{B}_{\delta_r}} \{|I(\mathbf{x})|\}.$$

Figure 6 (a) shows that only the circular antenna arrangement avoids ghost targets. The reason is the very dense synthetic antenna structure, see Figure 5. Figure 6 (b) shows that the ISLR and

the PSLR converges to a very good image quality. The alternating values come from the parallel sides of the even polygons. Thus, the circular arrangement achieves a very good image quality and suppresses all ghost targets in the scene.

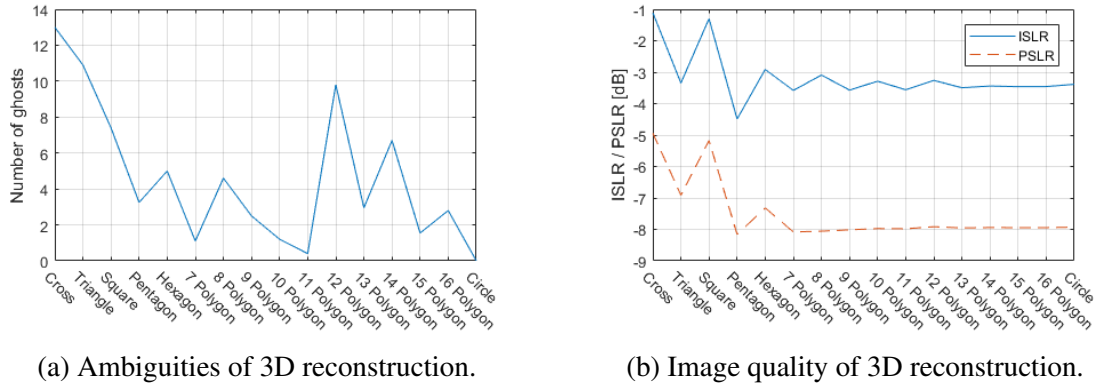


Figure 6: Results of different antenna arrangements. The number of ghost targets, ISLR and PSLR measure the quality of the 3D reconstruction. The circle antenna is the best one.

5. Simulation Results

To show the final outcome of this technique, we simulate a near-field road traffic situation, which consists of three lanes. On the road, two cars, one truck and several streetlights are simulated, see Figure 7 (a). Our car drives on the middle lane. All other objects in the scene are represented by several point reflectors. The raw data of the circular MISO radar system is generated by the superposition of the signals of all point reflectors by Equation (1). The result of the extended 3D backprojection reconstruction is shown in Figure 7 (b). It shows our car, the illumination area and the -7 dB isosurface of the whole reconstruction. The cars and even the streetlights can be seen in the Figure.

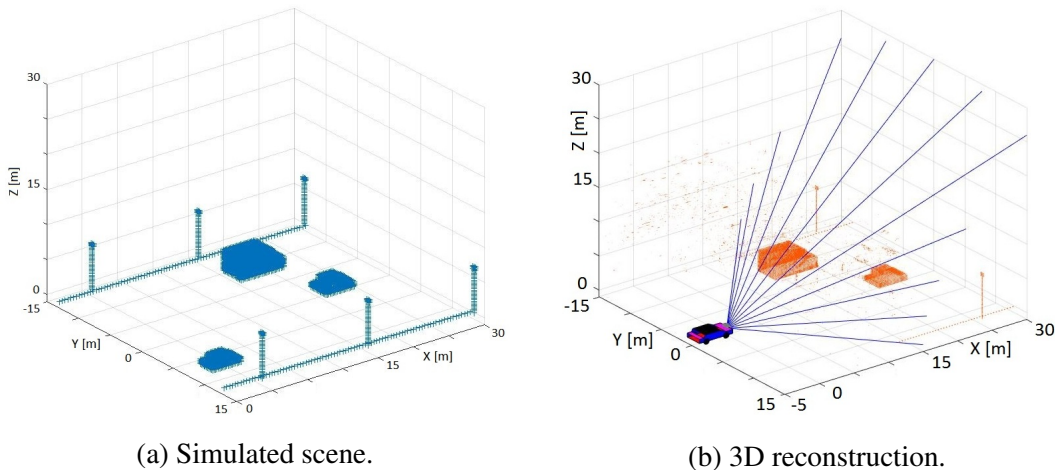


Figure 7: (a) Simulated point reflectors of two cars, one truck and several street lights, marked by blue crosses. (b) 3D reconstruction of the $\theta_{\text{ant}} = 90^\circ$ illumination area.

6. Conclusion

Because radar sensors work in all weather conditions, they are an inherent part of advanced driver assistance systems. Currently, a radar sensor mounted in front of a car scans different incident angles of the environment. This approach has the disadvantage of a low angular resolution. Hence, it has problems in near-field scenarios. However, to reconstruct the near-field environment of a car up to 30 m we apply the idea of synthetic aperture radar. Instead of moving one radar sensor along a straight line at the front of the car, we use several radar sensors. For a standard SISO 77 GHz system with 2 GHz bandwidth the distance between neighboring sensors has to be less than 1 mm. Otherwise, azimuth aliasing occurs in sense of ghost targets. We show that a MISO radar system with a circular 50 cm antenna increases the sensor distance from 1 mm to 4 cm without any loss of image quality. Simultaneously, this avoids azimuth aliasing and ambiguities. An extended MISO backprojection image formation algorithm is used to process a 3D image, which has the advantage to measure the height of objects. With this proposed algorithm the technique of synthetic aperture radar can be applied to measure the 3D near-field environment of a car with high angular resolution.

References

- [1] A. G. Stove, "Linear FMCW radar techniques", *IEE proceedings*, vol. 139, no.5, pp. 343-350, 1992.
- [2] Z. Tong, R. Renter, M. Fujimoto, "Fast chirp FMCW radar in automotive applications", *Radar Conference 2015, IET International*, 2015.
- [3] BMW Group Research and Technology, "RoCC - Radar on Chip for Car", *BMW Forschung und Technik GmbH*, München, 2012.
- [4] I. A. Cumming, F. H. Wong "Digital Processing of Synthetic Aperture Radar Data - Algorithms and Implementation", *Artech House*, Boston, 2005.
- [5] A. K. Loehner, "Improved azimuthal resolution of forward looking SAR by sophisticated antenna illumination function design", *IEE Proc. Radar, Sonar and Navigation*, vol. 145, pp. 128-134, 1998.
- [6] S. Dai, M. Liu, Y. Sun, W. Wiesbeck, "The latest development of high resolution imaging for forward looking SAR with multiple receiving antennas", in *Proc. IEEE IGARSS*, vol. 3, pp. 1433-1435, 2001.
- [7] J. Fortuny, "Efficient Algorithm for Three-Dimensional Near-Field Synthetic Apertur Radar Imaging", *Dissertation at University of Karlsruhe*, 2001.
- [8] A. Meta, "Signal Processing of FMCW Synthetic Aperture Radar Data", *Dissertation at Delft University of Technology*, 2006.
- [9] F. Fölster, "Erfassung ausgedehnter Objekte durch ein Automobil-Radar", *Shaker Verlag*, Aachen, 2007.
- [10] H. Winner, S. Hakuli, G. Wolf, "Handbuch Fahrerassistenzsysteme - Grundlagen, Komponenten und Systeme für aktive Sicherheit und Komfort", *Vieweg + Teubner Verlag*, Wiesbaden, 2012.
- [11] G. R. Curry, "Radar Essentials- A Concise Handbook for Radar Design and Performance Analysis", *Raleigh: ScieTech Publishing*, 2012.
- [12] L. A. Gorham, L. J. Moore, "SAR image formation toolbox for MATLAB", *Air force Research Laboratory*, 2010.
- [13] X. Lu, H. Sun, "Parameter assessment for SAR image quality evaluation system", in *Proc. 1st Asian and Pacific Conf. Synthetic Aperture Radar APSAR*, pp. 58-60, 2007.